Connections between sub-cloud coherent updrafts and the life cycle of maritime shallow cumulus clouds in large eddy simulation

Gu, J.-F. ORCID: https://orcid.org/0000-0002-7752-4553, Plant, R. S. ORCID: https://orcid.org/0000-0001-8808-0022 and Holloway, C. E. ORCID: https://orcid.org/0000-0001-9903-8989 (2024) Connections between sub-cloud coherent updrafts and the life cycle of maritime shallow cumulus clouds in large eddy simulation. Journal of Advances in Modeling Earth Systems, 16 (10). e2023MS003986. ISSN 1942-2466 doi: https://doi.org/10.1029/2023MS003986 Available at https://centaur.reading.ac.uk/118382/

JAMES | Journal of Advances in Modeling Earth Systems

RESEARCH ARTICLE
10.1029/2023MS003986

Connections Between Sub-Cloud Coherent Updrafts and the Life Cycle of Maritime Shallow Cumulus Clouds in Large Eddy Simulation

Jian-Feng Gu[1,2], **Robert S. Plant**[2], **and Christopher E. Holloway**[2]

[1]School of Atmospheric Sciences, Nanjing University, Nanjing, China, [2]Department of Meteorology, University of Reading, Reading, UK

Key Points:

- The evolution of maritime shallow cloud properties during the life cycle is connected to the activity of sub-cloud coherent structures
- Clouds are likely to be triggered by the humid faster growing sub-cloud coherent structures and start to dissipate without their ongoing support
- The evolution of cloud base mass-flux depends on cloud lifetime and is asymmetric around the middle of life for short and mid-lived clouds

Correspondence to:

J.-F. Gu,
jfgu@nju.edu.cn

Citation:

Gu, J.-F., Plant, R. S., & Holloway, C. E. (2024). Connections between sub-cloud coherent updrafts and the life cycle of maritime shallow cumulus clouds in large eddy simulation. *Journal of Advances in Modeling Earth Systems*, *16*, e2023MS003986. https://doi.org/10.1029/2023MS003986

Received 7 SEP 2023
Accepted 7 SEP 2024

Author Contributions:

Conceptualization: Jian-Feng Gu
Data curation: Jian-Feng Gu
Formal analysis: Jian-Feng Gu
Funding acquisition: Robert S. Plant, Christopher E. Holloway
Investigation: Jian-Feng Gu, Robert S. Plant, Christopher E. Holloway
Methodology: Jian-Feng Gu
Supervision: Jian-Feng Gu
Validation: Jian-Feng Gu
Visualization: Jian-Feng Gu
Writing – original draft: Jian-Feng Gu
Writing – review & editing: Jian-Feng Gu, Robert S. Plant, Christopher E. Holloway

Abstract We develop a novel approach to detect cloud-subcloud coupling during the cloud life cycle and analyze a large eddy simulation of marine shallow cumulus based on the Barbados oceanographic and meteorological experiment campaign. Our results demonstrate how the activity of sub-cloud coherent updrafts (SCUs) affect the evolution of shallow cloud properties during their life cycles, from triggering to development, and through to dissipation. Most clouds (~80%) are related to SCUs during their lifetime but not every SCU (~20% for short-lived ones) leads to cloud formation. The fastest growing SCUs in a relatively moist region are most likely to initiate clouds. The evolution of cloud base mass-flux depends on cloud lifetime. Compared with short-lived clouds, longer lived clouds have longer periods of development, even normalized by the full lifetime, and tend to increase their cloud base mass-flux to a stronger maximum. This is consistent with the evolution of mass flux near the top of SCU, indicating that the development of clouds is closely related to the sub-cloud activity. When the SCUs decay and detach from the lifting condensation level, the corresponding cloud base starts to rise, signifying the start of cloud dissipation, during which the cloud top lowers to approach the rising cloud base. Previous studies have described similar conceptual pieces of this relationship but here we provide a continuous framework to cover all the stages of cloud-subcloud coupling. Our findings provide quantitative evidence to supplement the conceptual model of shallow cloud life cycle and is critical to improve the steady-state assumption in parameterization.

Plain Language Summary The coupling between shallow trade wind cumulus clouds and sub-cloud processes is not well understood and remains one of the roadblocks to improving our climate modeling capability. As model resolution increases, the steady-state assumption adopted in conventional convection schemes no longer holds and the knowledge about the evolution of clouds is necessary to improve the parameterization. Observations have provided evidence of sub-cloud coherent updrafts being the roots of shallow clouds, but it is currently not practical to continuously detect how the shallow clouds evolve alongside the sub-cloud coherent structures. Our study takes a step forward to demonstrate how the sub-cloud coherent structures interact with the shallow clouds. It is shown that the evolution of sub-cloud coherent structures plays an important role from cloud initiation, development and through to dissipation. The comprehensive physical picture of the whole cloud life cycle uncovered in this study provides useful insights to improve the representation of cloud evolution in convection parameterizations with an explicit treatment of the cloud life cycle in the future.

1. Introduction

Shallow trade wind cumulus clouds dominate the redistribution of heat and moisture in the lower troposphere over most of the sub-tropical oceans. The strength of lower-tropospheric convective mixing can affect the low-cloud fraction, which is critical for the Earth's climate through its impact on reflected incoming solar radiation. However, due to our incomplete understanding of the highly turbulent flows and the complicated interactions across scales, convection parameterizations in climate models still have difficulties in representing low-cloud processes (Brient et al., 2016; Sherwood et al., 2014; Vial et al., 2016, 2017). This uncertainty is an important contribution toward the large spread of Equilibrium Climate Sensitivity (ECS) in climate models (Bony & Dufresne, 2005; Vial et al., 2013; Zelinka et al., 2020), indicating the necessity for a more in-depth understanding of shallow cumulus clouds (Vial et al., 2017).

One of the key processes that affects the dynamics of shallow cumulus clouds is the coupling with the sub-cloud layer (Grant, 2006). The behavior of shallow cumulus clouds is related to the turbulent sub-cloud layer because clouds result from sub-cloud coherent structures that reach the lifting condensation level (LCL). The relationship of such clouds to the sub-cloud fluxes and structure was well documented in early aircraft observations of several cases (LeMone & Pennell, 1976; Nicholls & LeMone, 1980). Using Doppler lidar observations, Lareau et al. (2018) showed that shallow cumulus clouds are linked to coherent updrafts extending over the depth of the sub-cloud layer. The dependence of vertical velocity and moisture structure of cumulus clouds and their associated sub-cloud circulations on the size, shape and orientation of surface-connected coherent structures was reported in large eddy simulations of shallow convective clouds (Denby et al., 2022; Griewank et al., 2020, 2022). Zheng et al. (2021) demonstrated that half of the variability in the ensemble-mean cloud-base vertical velocity can be explained by the ensemble properties of sub-cloud turbulence. A close connection between sub-cloud turbulent flows and shallow cumulus clouds has been incorporated into convection parameterization schemes with empirically derived relationships between cloud base vertical velocity and sub-cloud turbulence intensity (Betts, 1973; Fletcher & Bretherton, 2010; Neggers et al., 2006; Stevens, 2006; Zheng, 2019). This is important for estimating the cloud-base mass flux and coupling with microphysical processes. The transition across scales from turbulent flows, to sub-cloud coherent structures and to shallow cumulus clouds forms the basis of developing convection parameterization schemes that intend to unify the representation of boundary layer turbulence and moist convection (Golaz et al., 2002; Larson, 2017; Larson & Golaz, 2005; Larson et al., 2002; Neggers, 2015; Rio & Hourdin, 2008; Siebesma et al., 2007; Soares et al., 2004; Suselj et al., 2012, 2019; Tan et al., 2018).

Comprehensive understanding of the coupling between the sub-cloud layer and trade wind cumulus clouds also needs more in-depth investigation into how the sub-cloud processes affect the life cycle of shallow clouds. Considering the effect of cloud life cycle could allow improvement of convection schemes (Cho, 1977; Kain, 2004; Neggers & Griewank, 2021). Most schemes use a steady-state cloud model while in reality the clouds may evolve through pulse-like events (Blyth et al., 2005; Heus et al., 2009; Scorer & Ludlam, 1953; Zhao & Austin, 2005a, 2005b) and so with cloud properties that can vary significantly depending on the stage of development (S. S. Chen & Houze Jr, 1997). Such evolution may be important for capturing related events, such as the transition from shallow clouds to deep clouds (Kairoutdinov & Randall, 2002; Kuang & Bretherton, 2006) and spatial organization into convective clusters (Neggers & Griewank, 2021, 2022). Neggers and Griewank (2021) recently developed a binominal population model that accounts for the pulse-like behavior and further coupled the model to the eddy-diffusivity mass-flux (EDMF) framework (Neggers & Griewank, 2022), yielding a decentralized convection scheme that provides insights into impacts of spatial organization on convective transport. However, parameterizations of cloud life cycle usually hypothesize the evolution of cloud properties (Neggers & Griewank, 2021; Sakradzija et al., 2015) due to a lack of direct information. Therefore, it is necessary to make a systematic examination into how the dynamical and thermodynamic processes in the sub-cloud layer can affect the full cycle of triggering, development and dissipation of clouds, which will provide useful guidance to improve the steady-state assumption adopted in the conventional convection parameterizations.

Ground-based observations, such as Doppler lidar, are able to detect sub-cloud-layer structures below shallow clouds, but cannot continuously track them to cover the whole life cycle of clouds because the lidar measures only a few places and times for individual clouds. Geostationary satellite observations have the advantage of capturing the evolution of clouds over their lifetime but may not have enough spatial resolution to detect the detailed structures and most importantly do not have information in the sub-cloud layer to infer the coupling between clouds and the sub-cloud layer coherent structures (Seelig et al., 2021). Stereo photogrammetry (Romps & Öktem, 2018; Romps et al., 2021; Öktem et al., 2014), while being able to collect detailed cloud properties (e.g., cloud depth, cloud height) over the life cycle, shares a similar problem with the geostationary satellite observations in that no matching information for the sub-cloud layer is available. Furthermore, these observations do not provide details of cloud and sub-cloud coupling over the ocean.

High-resolution large-eddy simulations provide an alternative route for understanding the dynamics of the cloud life cycle in the absence of continuous monitoring over the ocean, because they are able to resolve most of the energetic turbulent flows that are responsible for the evolution of moist convection (Siebesma & Cuijpers, 1995; Siebesma & Jonker, 2000; Siebesma et al., 2003). By tracking the life cycle of six clouds in a large eddy simulation of trade wind cumulus clouds with a uniform resolution of 25 m, Zhao and Austin (2005b), (2005a)

demonstrated that the combined effects of small and large clouds are essential for heat and moisture transport to achieve an equilibrium state with the large-scale forcing. They also showed that shedding thermals are critical to explain the dynamics of mixing between clouds and the environment. Heus et al. (2009) combined automated constraints and a three-dimensional virtual reality environment to select a considerable number of exemplary clouds throughout their lifetime, and provided robust statistical results to illustrate the fundamental role of pulses/thermals in cloud evolution. Nevertheless, these studies have limitations for our present purposes, either due to the limited sampling (Zhao & Austin, 2005a, 2005b) or a focus other than the links between sub-cloud coherent structures and cloud evolution (Dawe & Austin, 2012; Heus & Seifert, 2013; Heus et al., 2009; Jiang et al., 2006; Plant, 2009).

In this study, we will investigate how the life cycle of shallow cumulus clouds is affected by the evolution of sub-cloud coherent structures, using a high-resolution large eddy simulation of a typical trade wind shallow cumulus case with simple forcings and no precipitation. The rest of the paper is organized as follows. Section 2 will present the details of the simulation and the methodology used to identify and track the sub-cloud coherent structures and cloud over the life cycle, and to make links between them. Section 3 will address the evolution of cloud properties and investigate the possible role of sub-cloud coherent structures during the life cycle. Evidence will be provided in Sections 4 and 5 to illustrate how the initiation and decay of clouds is affected by properties of sub-cloud coherent structures. The possible factors that affect the length of cloud lifetime will be explored in Section 6. Discussion and conclusions will be given in Section 7.

2. Simulation and Methodology

2.1. Large Eddy Simulation

The Met Office-NERC (Natural Environment Research Council) Cloud (N. Brown et al., 2015; N. Brown et al., 2018, MONC) model is used to perform a large-eddy simulation of shallow trade wind cumulus clouds over sub-tropical ocean, based on the Barbados Oceanographic and Meteorological Experiment (BOMEX). The BOMEX case has been widely studied for maritime non-precipitating shallow cumulus clouds. It fits well with the purpose of this study that aims to investigate the coupling between sub-cloud coherent structures and life cycle of maritime clouds, which is not achievable by ground-based observations in land. The model configuration follows that of Gu et al. (2020). The grid spacing is 25 m in all directions and the domain size is $(6.4\ \mathrm{km})^2$ in the horizontal and 3 km in the vertical. Sub-grid turbulence is parameterized with the 3D Smagorinsky-Lilly scheme (Lilly, 1962; Smagorinsky, 1963). A simple saturation-adjustment cloud scheme is used to represent the conversion between water vapor and cloud liquid water as this is a non-precipitating case without ice species. While previous studies have shown that cloud statistics can be affected by microphysics (Endo et al., 2019; Zhang et al., 2017), the simple saturation-adjustment scheme is chosen here to ensure minimal physics complexity and therefore the results focus on connections between sub-cloud layer coherent structures and cloud life cycles that are essentially dynamics-driven. Our analyses cover a period in the equilibrium state from hour $5-7$ during the simulation, with 1 min output frequency for an accurate continuous tracking of cloud objects and the sub-cloud coherent structures.

2.2. Object Identification and Tracking

2.2.1. Object Identification

In the simulation, the cloudy points are identified where the mixing ratio of cloud liquid water exceeds 10^{-5} kg kg^{-1}. A cloud object is a collection of spatially adjacent grid points each of which satisfies the above criterion: that is, contiguous grid points are identified as an individual object by checking the neighboring 8 grid points around the cloudy points until no more cloudy points are found.

Following Couvreux et al. (2010), we use a passive tracer for conditional sampling of coherent updrafts below the level of cloud base. The passive tracer is emitted from the surface with a constant surface flux and undergoes a radioactive decay at a constant time scale (τ_0):

$$\frac{\partial C}{\partial t} = -\frac{C}{\tau_0} \tag{1}$$

The grid points considered to form part of the sub-cloud coherent updrafts (SCU) are identified with the following conditions:

$$x \in SCU \text{ if } C' > m \times \max(\sigma_C, \sigma_{\min}) \ \& \ w > 0, \tag{2}$$

where C' is the anomaly of the tracer concentration with respect to the domain mean at each vertical level and w is the vertical velocity. m is a scaling factor and is set to 1 for most of the results discussed below. σ_C and $\sigma_{\min}$ are the standard deviation of tracer concentration at the given level and the minimum threshold, respectively. $\sigma_{\min}$ is calculated as 5% of the averaged standard deviation below the corresponding vertical level. Using these conditions, the most energetic coherent updrafts can be effectively found and will be used to understand the connection with cloud life cycles. The robustness of the results in Section 3 are further examined by testing the sensitivity to the scaling factor and the way that the surface flux of the passive tracer is prescribed.

It should be emphasized that the coherent structures are closely packed near the surface, where these structures start to form. The tracer concentration anomalies near the surface are small because the coherent structures have not fully developed yet. This leads to a difficulty in effectively distinguishing different coherent structure objects and to link each cloud in any simple and reliable manner with a single sub-cloud coherent structure. To separate the individual coherent structures, we only apply the conditional sampling between the heights of 250 and 600 m. The 250 m level is chosen because the horizontal scale of the auto-correlation of vertical velocity is largest there (Gu, Plant, Holloway, & Clark, 2024) so that the sub-cloud coherent structures can be clearly distinguished. The 600 m level is slightly above the cloud base and thus the sub-cloud coherent structures and the clouds will not be confused. Another consideration is that the sub-cloud coherent structure detaches from the cloud during the decaying stage of the cloud, as shown in Sec 4. We choose 600 m in order to identify such detachments reliably. This height level is slightly above the cloud base so that the detachment of the sub-cloud coherent structure can be easily detected once the associated tracer becomes restricted to the sub-cloud layer. After the SCU grid points are determined, the individual coherent structures are identified, following the same strategy as for the cloud objects.

2.2.2. Object Tracking

Continuous records of properties during the lifetime are necessary for understanding the life cycle, requiring a continuous tracking of the objects. After the cloud objects and the sub-cloud coherent structures at all output times have been identified following Section 2.2.1, a matching up of objects at adjacent output times is conducted. The matching algorithm follows that developed in Gu et al. (2020) and is an extension of Muetzelfeldt (2020), which itself combines methods from Stein et al. (2014) and Plant (2009), allowing it to track 3D objects instead of 2D objects.

The 3D objects are first projected vertically onto the horizontal plane. Using the projected 2D fields, a translation vector between one output time and the next is obtained using the convolution of Fourier-transformed 2D fields at the two adjacent output times, which produces the maximum correlation of the cloud fields. A particular object is then considered to be the same object from one output time to the next if, when projected forwards with the translation vector to the next output time, it overlaps with or is touching an object at the next output time. There are some complications when building up the life history, depending on how the projected objects overlap with those at next output time, which can result in merging and splitting of cloud objects (see Plant, 2009; Muetzelfeldt, 2020, for details). For convenience of analysis over the life cycle of each object, here we retain only one object if there are multiple objects identified as overlapping or touching. If one object merges with another, we continue to track both objects as one merged object until it dissipates. If an object splits into several objects, we only continue to track one object. The retained object has the closest depth to the parent one at previous output time. In this way, each object can be appropriately tracked over its lifetime without losing much information.

Figure 1 illustrates the tracking for three example clouds with different lifetimes. The tracks mostly follow a quasi-linear line due to the background mean flow of -8 ms^{-1} within the cloud layer. With this method, a total of 2,224 cloud objects have been tracked and subsampling tests confirm that this is sufficient to provide robust statistical results.

To study how shallow cumulus clouds are supported by sub-cloud coherent structures, and how the sub-cloud coherent structures affect the initiation, development and dissipation of shallow clouds, we must develop a

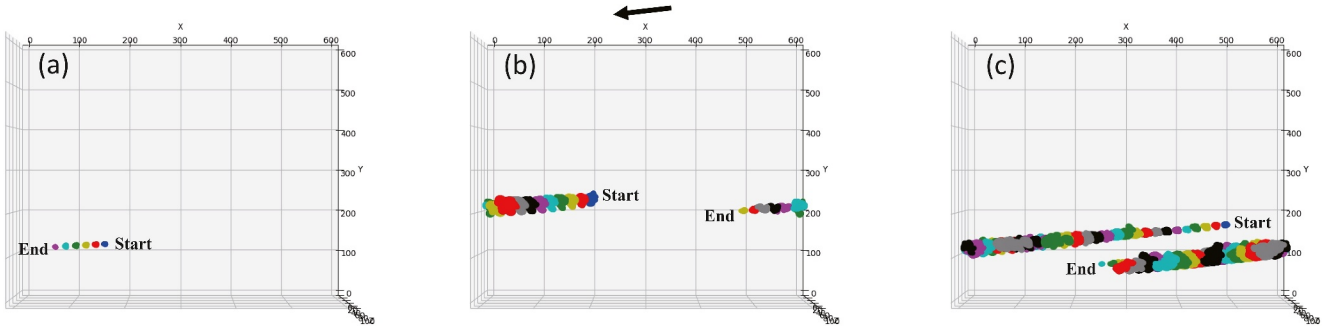

Figure 1. The tracks of three example clouds viewed from the top: (a) cloud 50, (b) cloud 1, and (c) cloud 222. The first cloud location of each track is marked with blue color. Red, yellow, green, cyan, magenta, black and gray colors are then used in a repeating sequence for the subsequent locations at 1 min intervals. The first and last cloud object during the tracked period are marked with bold "Start" and "End" on each panel. The black thick arrow above panel (b) denotes the mean flow direction near cloud base.

strategy to determine connections between the two object types. In principle, the passive tracer concentration could be used to make connections since the passive tracers are transported into the clouds. However, such a method would not be reliable: first, because the tracers will be detrained out of cloud and thus non-zero concentrations will occur in the environment and therefore cannot be used as a marker of clouds, and second because the connection might break when the sub-cloud coherent structure no longer supports the cloud. To this end, we determine whether a cloud overlaps with a sub-cloud coherent structure. At each time, a tracked cloud is associated with a sub-cloud coherent structure if some of its cloudy points are also occupied by the sub-cloud coherent structure.

The overlapping could be considered either in 3D or in 2D, as illustrated by the schematic diagram of Figure 2. In some cases, the sub-cloud coherent structure may have just started to develop and has not overshot the LCL, or it may have started to decay such that its top becomes detached from the cloud base. The base of the clouds may also rise. We wish to make an association in such cases, such that the sub-cloud coherent structures and the clouds remain connected while both object types complete their full life cycle. Given these considerations, a sub-cloud coherent structure and a cloud are marked as connected if the vertically projected 2D fields from their 3D objects overlap even though they may not have overlap in the vertical (e.g., bottom row of Figure 2). This approach ensures the collection of information over the full life cycle for a comprehensive evaluation of interactions between the sub-cloud coherent structures and the shallow cumulus clouds.

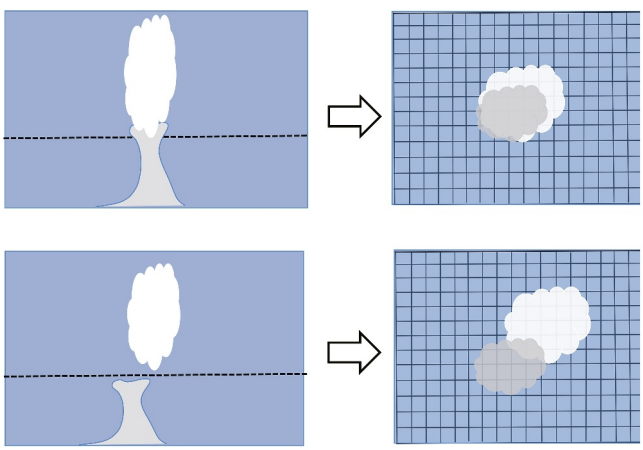

Figure 2. Schematic diagram of the strategy to connect sub-cloud coherent structures and cloud objects. The upper row represents the overlap of a sub-cloud coherent structure and a cloud object in the *xz* (left) and *xy* (right) planes. The lower row represents a situation in which a sub-cloud coherent structure does not overlap with a cloud object in the *xz* plane (left) but which can be connected if projected onto the *xy* plane (right). The white color marks the cloud object and the gray color marks the sub-cloud coherent structure. The horizontal dotted line represents the lifting condensation level.

3. Cloud Properties Over Life Cycle

Before presenting details of the cloud life cycle, it is very interesting to see the extent to which the clouds have support from sub-cloud processes. Figure 3 shows the normalized frequency distribution of cloud lifetime, along with the proportion of clouds that have connections with sub-cloud coherent structures as a function of the lifetime. The lifetime distribution has a maximum of 78% for the shortest lived clouds (5–10 min) and decays approximately exponentially as the cloud lifetime increases. The longest lived cloud has a lifetime around 45 min. Such long-lived shallow cumulus clouds have been observed, and also previously found within large eddy simulations (Neggers et al., 2003; Romps et al., 2021). A cloud is accounted as having support from SCU structures if it is found to connect with an SCU at any time during the life cycle. Not every cloud has sub-cloud support, especially the short-lived ones. Only ∼80% of the short-lived clouds are connected with sub-cloud coherent structures, although this proportion increases to nearly 100% for long-lived clouds. The absence of sub-cloud support for some short-lived clouds may indicate that these are dynamically passive, or else that some of the clouds in the data set were captured only during the later part of their decaying phase, at

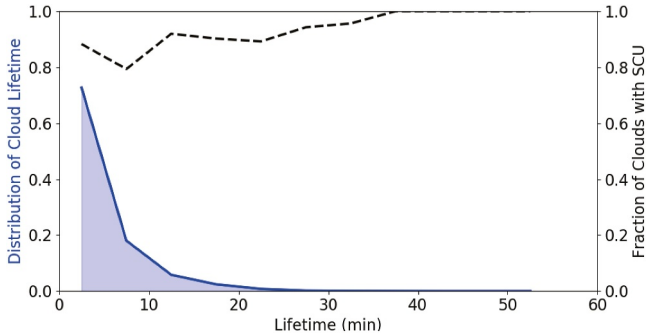

Figure 3. The frequency distribution of cloud lifetime is shown with blue shading, for a bin size of 5 min and subject to a minimum lifetime of 5 min. The black dashed line represents the proportion of clouds that have a connected sub-cloud updraft at some stage during their life cycle.

which time associated sub-cloud coherent structures may have disappeared. Nonetheless, Figure 3 clearly shows that connected sub-cloud coherent structures must exist to support a long life cycle, consistent with previous studies (Lareau et al., 2018; LeMone & Pennell, 1976; LeMone et al., 2019; van Stratum et al., 2014).

Figure 4 shows the evolution of cloud top, cloud base (Figure 4a) and cloud depth (Figure 4b) during the life cycle. The clouds have been divided into three groups: short-lived (5−10min), mid-lived (10−15min) and long-lived (>15min) clouds, based on their lifetime. Clouds with lifetimes less than 5 min are excluded to minimize the impact from passive clouds. To facilitate comparison of the evolution for clouds with different lifetimes, each cloud life cycle has been normalized before compositing, with cloud properties interpolated onto the relative lifetime and then averaged for each group. The mean cloud bases start from the lifting condensation level (LCL; ∼540m) no matter how long the clouds last. The mean cloud top starts from a level that is about 125 m above the mean cloud base, steadily elevates to achieve a maximum before descending. In the later part of the life cycle, the mean cloud top and cloud base approach each other with the rise of cloud base being more marked than the fall in cloud top. The cycle of cloud depth is largely determined by cloud top changes in the first part of the cycle and by cloud base changes at the end. The non-zero cloud depth at the beginning and the end indicates that the clouds initiate and dissipate rapidly as the model output interval is only 1 min. The absence of a plateau in the time series of cloud properties indicates that the clouds are more bubble-like clouds, rather than plume-like clouds with a steady state. These general features are consistent with stereo photogrammetry observations and other large eddy simulations of shallow cumulus clouds on land (Romps et al., 2021; J. Chen et al., 2023).

Nevertheless, the evolution of cloud properties has significant differences among clouds of different duration. The mean cloud top of short-lived clouds is higher than the other two groups of clouds at the beginning, perhaps because some of these clouds have developed for a while before the tracking period (hour 5–7) begins. Another possibility is that there might be some sub-cloud coherent structures pulsing intermittently across the LCL, thus having higher cloud top when first detected as a connection, but not lasting too long. The evolution of cloud top and cloud depth are not symmetric over the normalized lifetime and differs for the three cloud groups. The top of the short-lived clouds only takes 50% of the life cycle to rise to its maximum before it gradually descends. The top of the longest lived clouds rises the most (from 650 to 1,300 m) in the normalized lifetime during the development stage. Their tops reach the highest level at around 80% of the life cycle, similar to the mid-lived clouds. The cloud

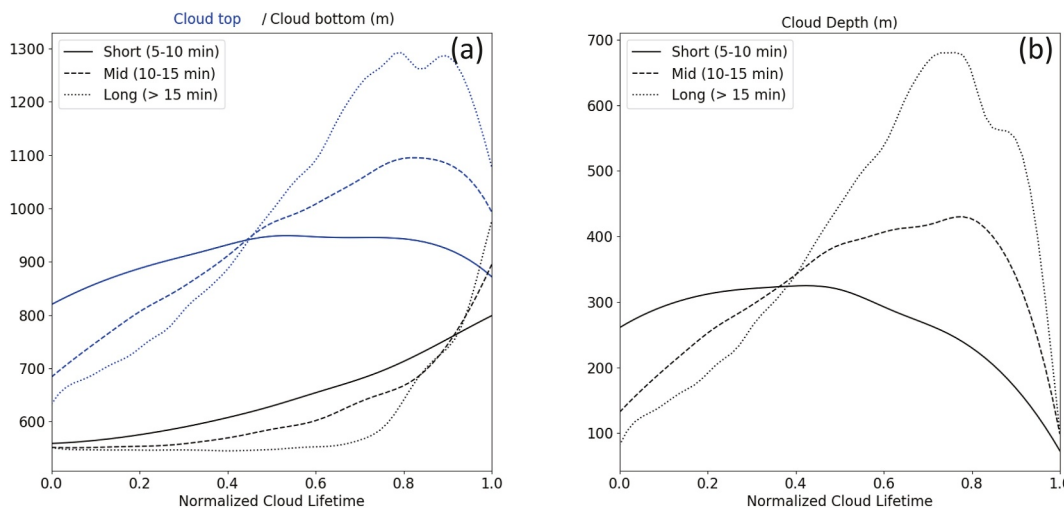

Figure 4. Evolution of (a) cloud top (blue lines) and cloud base (black lines) and (b) cloud depth (black lines) with normalized cloud lifetime. The clouds are divided into three groups based on the length of the lifetime. The solid lines represent short-lived clouds with lifetimes of 5−10 min, the dashed lines represent mid-lived clouds with lifetime of 10−15 min and the dotted lines represent long-lived clouds with lifetime longer than 15 min.

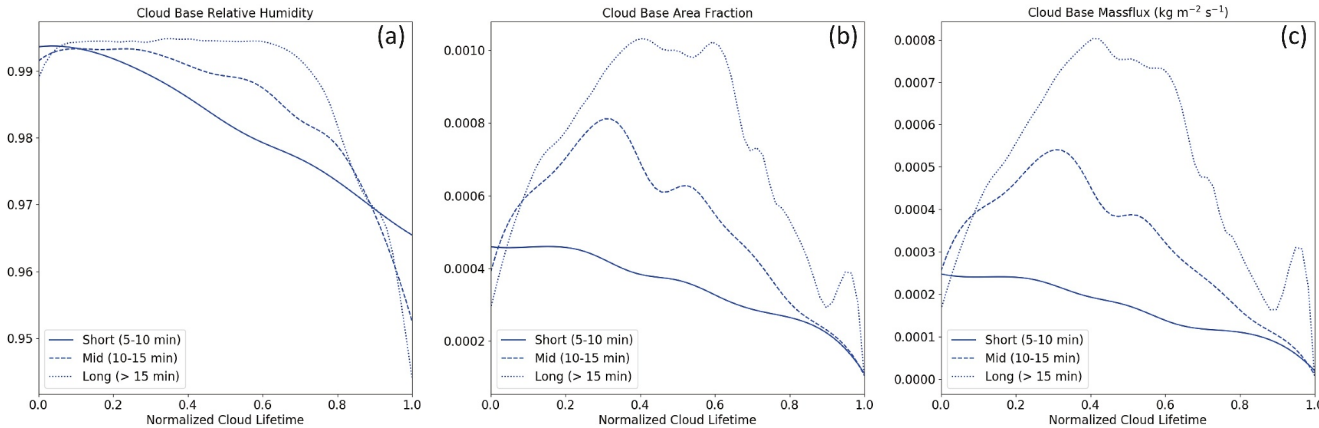

Figure 5. Evolution of (a) cloud base relative humidity, (b) cloud base area fraction and (c) cloud base mass-flux (kgm^{-2}s^{-1}), with normalized cloud lifetime. The solid, dashed and dotted lines represent the same groups of clouds that have sub-cloud coherent updrafts attached at each normalized lifetime as in Figure 4.

tops of mid-lived and long-lived clouds both decrease quickly during the last stage. The longer the clouds live, the later their bases start to rise. The cloud base of short-lived ones starts to rise from the very beginning. The mid-lived ones' bases start to rise at around 20% of the lifetime while the base of the long-lived clouds does not appear to rise until they have gone through 60% of the lifetime. In summary, long-lived clouds tend to have larger depth. The longer a cloud lives, the faster its top rises and the later its base starts to rise. These results indicate that different types of cloud property evolution should be considered in a spectral plume model if the cloud life cycle needs to be parameterized.

In addition to the vertical extent of the cloud base, other properties, such as relative humidity and the cloud-base mass flux, are also important for us to understand the dynamics. Figure 5a shows the evolution of relative humidity at the LCL during the whole cloud life cycle. The relative humidity of all clouds starts at near saturation but that of the short-lived ones decreases almost immediately. The relative humidity at LCL for mid-lived and long-lived clouds remains steady until their respective cloud base begins to rise. The timing for the decrease of relative humidity is consistent with the rise of cloud base, as shown in Figure 4. Similar aspects of evolution can be seen for the cloud-base mass flux (Figure 5b), with decreasing mass flux from the beginning for short-lived clouds and an increasing and decaying cycle for mid-lived and long-lived clouds. The evolution of cloud-base mass flux is largely controlled by the cloud-base area fraction (compare Figures 5b and 5c), regardless of the length of cloud lifetime. The initial cloud-base mass fluxes among the different cloud groups are close to each other and clearly larger than zero, pointing to the importance of dynamical support from below when the clouds are initiated. Comparing Figures 5a and 5b shows that the relative humidity near cloud base starts to decrease later within the life cycle for the larger clouds. This might be because a larger cloud area can protect the moisture from dilution, thus leading to a longer cloud lifetime.

4. Role of Sub-Cloud Coherent Structure During the Life Cycle

To examine the role of sub-cloud coherent structures on the cloud life cycle, we consider the contribution of the resolved vertical velocity variance to the turbulent kinetic energy (TKE) at the LCL: that is, $(1/2)\overline{w'^2}$. The variance is evaluated for the sub-cloud coherent structures that are connected with each cloud during its life cycle, and is averaged for each group of clouds and interpolated onto the normalized cloud lifetime (Figure 6). The main features of the variance evolution for different groups of clouds are consistent with those of cloud base mass-flux. The value at LCL starts from non-zero, indicating that the sub-cloud coherent structures have already developed to a certain strength when the cloud is first formed. The SCU variance below mid-lived clouds increases to a maximum only when 20% of the life cycle has passed while that below long-lived clouds achieves a maximum at 40% of the normalized lifetime. Comparing Figures 4a and 6, the timing for the sub-cloud coherent structures below mid-lived and long-lived clouds to achieve maximum variance occurs ahead of the timing for the rise of cloud base. Since the rise of cloud base signifies the start of cloud dissipation, the earlier start to the decay of SCU

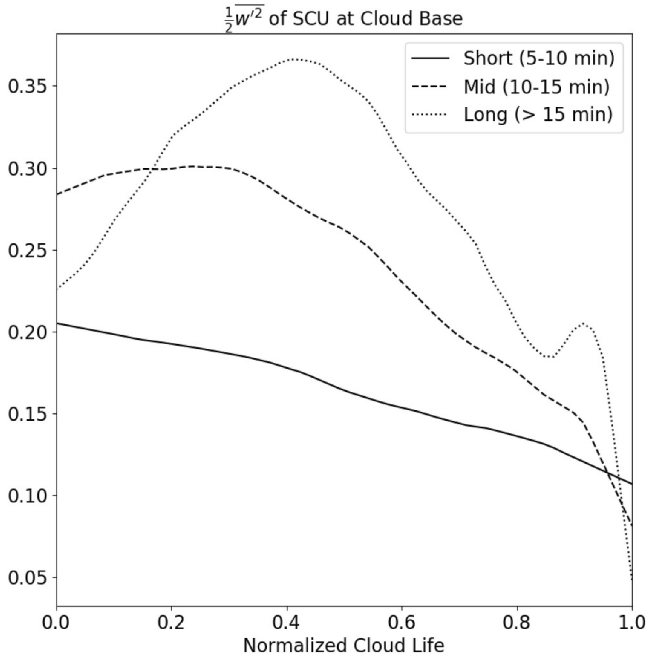

Figure 6. Evolution of sub-cloud coherent updrafts' resolved vertical velocity variance ($(1/2)\overline{w'^2}$, m^2s^{-2}) at cloud base with normalized cloud lifetime. The solid, dashed and dotted lines represent the same groups of clouds as in Figure 4.

variance strongly supports the idea that dynamical forcing from the sub-cloud coherent structures is a key process that supports the development and maintenance of cloud life cycle.

We further illustrate the critical role of sub-cloud coherent structures during the cloud lifetime by examining several examples. Figure 7 shows the whole life cycle for three example clouds, one in each group. For each cloud, a sub-cloud coherent structure is found below the LCL at the start of the life cycle. It is when the SCU disappears in the sub-cloud layer that the cloud base starts to rise, consistent with the average behavior shown in Figure 6. The cloud top stops ascending and begins to lower shortly after the rise of cloud base (Figure 7c), indicating that the cloud ceases development because of the lack of support from below. While the physical picture of cloud evolution has been well established in previous studies (e.g., Heus & Seifert, 2013; Heus et al., 2009; Romps et al., 2021; Zhao & Austin, 2005a, 2005b), our study provides the first explicit evidence to illustrate how cloud-subcloud coupling affects shallow cumulus clouds during different stages of the cloud life cycle.

5. Cloud Triggering

Sub-cloud coherent structures do not always lead to the formation of clouds, even though they are necessary during the cloud life cycle (LeMone & Pennell, 1976; Lareau et al., 2018; van Stratum et al., 2014; Wang et al., 2022). Figure 8 shows the frequency distributions of lifetime for all the tracked sub-cloud coherent structures (blue shading) and for those that are connected to clouds during their lifetime (red shading). Both distributions decrease approximately exponentially with lifetime, consistent with that of cloud lifetime distribution (Figure 1). Short-lived SCUs are less likely to support the formation of a cloud (LeMone & Pennell, 1976, LeMone et al., 2019). The percentage of sub-cloud coherent updrafts that are connected to clouds increases non-linearly from only 20% when the lifetime is less than 5 min to almost 100% when the lifetime is longer than 30 min, indicating the favorable role of long-lived SCU for cloud formation. The non-linear increase of the percentage of SCUs supporting shallow clouds with SCUs' lifetime might result from the positive feedback between the SCUs and the shallow cumulus clouds, that is, the presence of cloud can lead to a larger lifetime of SCU through enhanced venting and sub-cloud mixing, as found in Williams et al. (2011). But what determines whether a SCU will initiate a cloud?

In most mass-flux-based convection parameterizations, the triggering of convection depends on the thermodynamic conditions, particularly the buoyancy of an adiabatic ascending parcel rising from surface or mixed layer to the LCL (e.g., Gregory & Rowntree, 1990). Dynamical forcing, such as the grid-scale convergence or the vertical velocity contribution to TKE, may also be considered in the trigger function (e.g., Kain, 2004). Some schemes

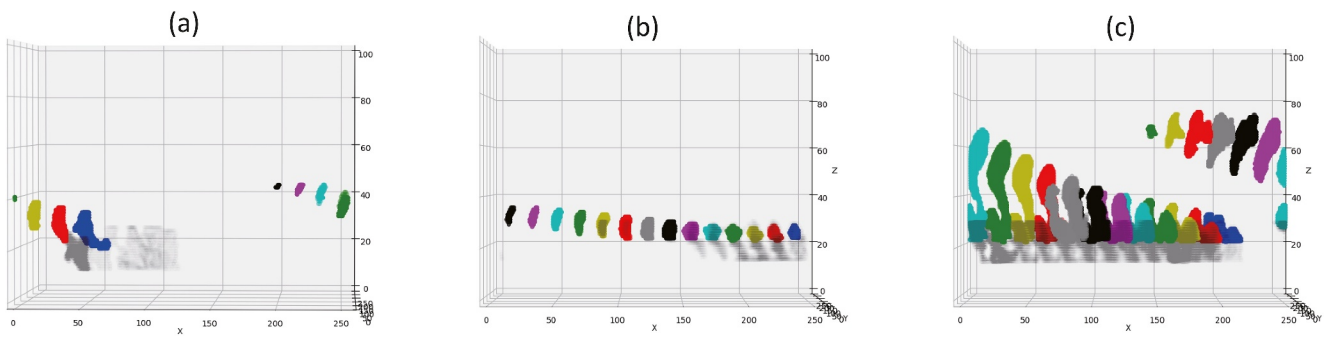

Figure 7. Side view of the tracks of three representative clouds with lifetimes of (a) 7 min, (b) 14 min, and (c) 18 min, corresponding to the short-lived, mid-lived and long-lived clouds, respectively. The first cloud location of each track is marked with blue. Red, yellow, green, cyan, magenta, black and gray colors are then used in a repeating sequence for the subsequent locations at 1 min intervals. The gray color represents the corresponding sequence of locations for the sub-cloud coherent updrafts.

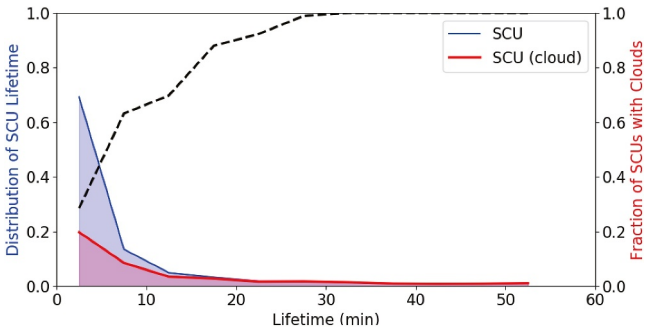

Figure 8. The frequency distribution of lifetime of tracked sub-cloud coherent updrafts (SCUs), for a bin size of 5 min and subject to a minimum lifetime of 5 min. The blue shading represents the distribution of all SCUs. The red shading represents the distribution of the SCUs that lead to the formation of clouds. The black dashed line represents the proportion of SCUs associated with cloud formation.

consider a combination of both thermodynamic and dynamical forcings to have a more comprehensive representation of initiation (e.g., Xie et al., 2004). Therefore, it is of interest to test whether the mean strength and the buoyancy of the sub-cloud coherent structure are indeed important factors for cloud initiation.

Figure 9 shows the life-cycle-mean buoyancy (virtual potential temperature perturbation, Figure 9a), vertical velocity variance (Figure 9b) and vertical velocity (Figure 9c) within the sub-cloud coherent structures that do and do not form clouds as a function of SCU lifetime. It is perhaps a surprise that the mean buoyancy does not indicate whether a cloud will form from a sub-cloud coherent structure, because the mean buoyancy is generally negative for all SCU and the buoyancy of SCU associated with clouds is more negative than that of SCU not supporting clouds (Figure 9a). However, both the variance and mean of the vertical velocity in the SCU associated with clouds are larger than those not supporting clouds (Figures 9b and 9c), suggesting that continuous dynamical support from the SCU below is more important than favorable local thermodynamic conditions for cloud formation.

However, the life-cycle-mean vertical velocity and variance can not be viewed as precursors for the initiation of clouds. To see whether these SCU variables might provide useful predictors for cloud formation, Figure 10 shows the vertical velocity, variance and buoyancy within the sub-cloud coherent structures when clouds form. The differences in vertical velocity for most lifetime bins are not significant enough to distinguish the SCUs that do or do not lead to clouds (Figure 10c). The initial vertical velocity variance for the SCUs associated with clouds is generally larger than that for the SCUs not supporting clouds, except when the lifetime of SCUs is between 20 and 25 min (Figure 10b). The initial buoyancy again does not have useful information to predict the cloud formation as it is larger for SCUs that do not produce clouds, regardless of the sign of the buoyancy (Figure 10a).

To establish why the SCUs that form clouds do not have favorable buoyancy, we examine the initial relative humidity perturbation (Figure 11a). It is found that the initial relative humidity perturbation of the SCUs that support cloud formation is clearly larger than those that do not, indicating that such updrafts are moister but must be colder (since warmer updrafts together with higher relative humidity would imply larger buoyancy, in contradiction with Figures 9a and 10a). It should be noted that the negative buoyancy of cloudy SCUs shown here is mostly due to the averaging over the entire sub-cloud coherent structures. The buoyancy within the SCUs should be positive in the lower part because most of the SCUs are driven by positive buoyancy from surface energy fluxes. The negative buoyancy come from the upper-part of the SCUs. Some SCUs (duration between 10 and 30 min) have positive buoyancy but do not support clouds, probably because of lower relative humidity resulted from high temperature (see Figure 11a).

Although the initial vertical velocity of SCUs is not a good predictor for cloud formation, its rate of change at the initiation time turns out to be a favorable factor. Figure 11b shows that for all the sub-cloud coherent structures with lifetimes longer than 5 min, the initial change of mean vertical velocity is positive for the SCUs that lead to cloud formation while it is negative for the SCUs that do not support clouds. The stronger mean vertical acceleration of these updrafts is also accompanied by more rapid growth of SCU volume. Figure 11c shows that the initial volume change is significantly larger if a sub-cloud coherent structure favors cloud formation, regardless of its lifetime. In short, a sub-cloud coherent structure is more likely to support cloud formation if it is initially dynamically faster growing with more rapid mean vertical acceleration. In addition to the dynamical condition, higher initial relative humidity, rather than the buoyancy, also favors the formation of clouds from sub-cloud coherent structures.

6. Cloud Lifetime

After the formation of cloud, how long it will last plays an important role in determining heat and moisture exchanges between the free troposphere and the boundary layer. As shown in Figure 5, longer-lived clouds have stronger cloud-base mass flux over most of the lifetime, suggesting that the cloud lifetime is connected to the dynamical support provided by the associated sub-cloud coherent structure. This idea is confirmed by Figure 12a which shows that cloud lifetime increases non-linearly with the life-mean cloud-base mass flux. The very short-

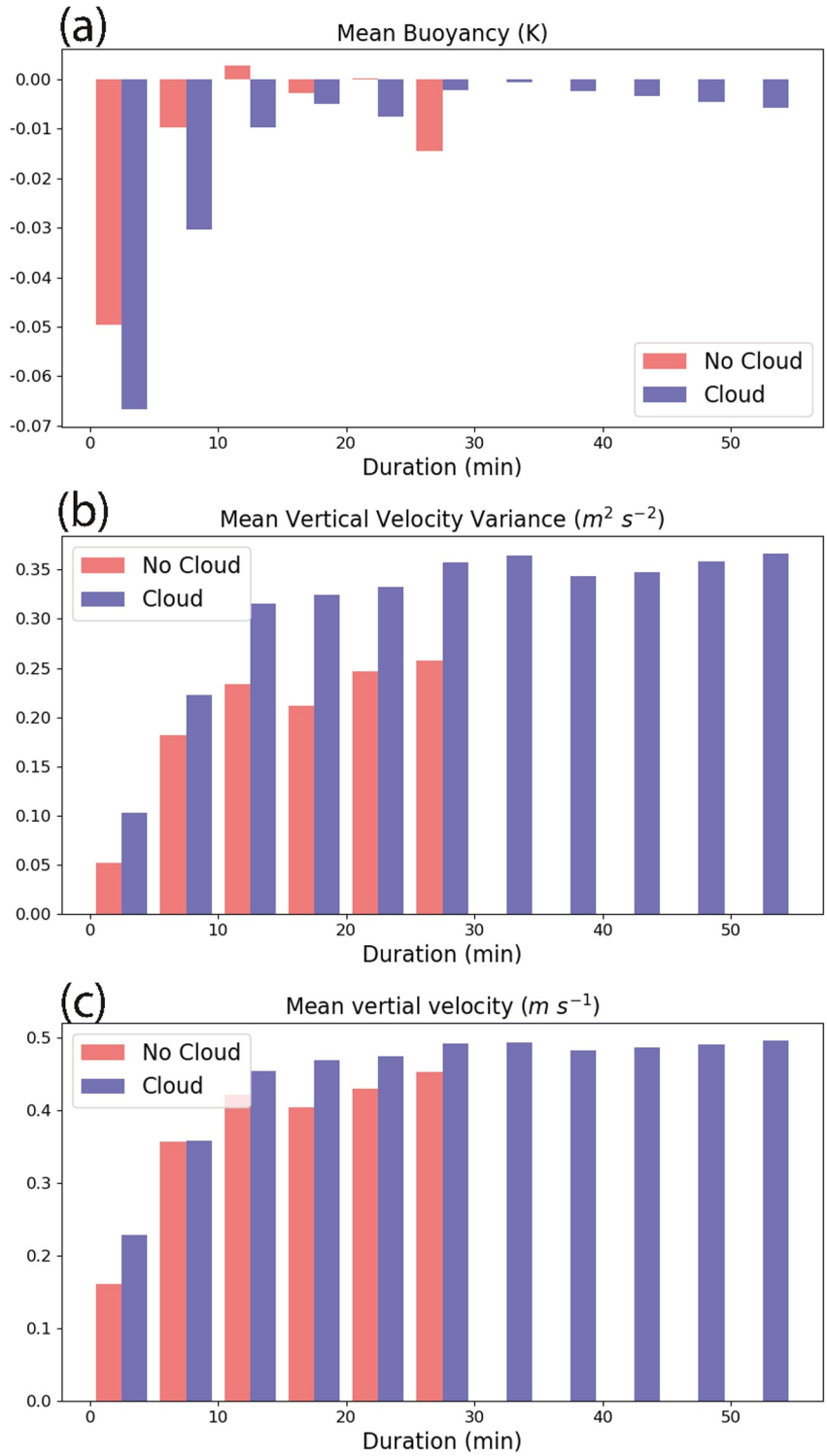

Figure 9. Life cycle mean distributions of (a) buoyancy (K), (b) vertical velocity variance ($(1/2)\overline{w'^2}$; m^2 s^{-2}) and (c) vertical velocity (m s^{-1}) of sub-cloud coherent updrafts (SCUs) that are (blue) or are not (red) associated with cloud formation. The buoyancy is calculated as the perturbation of virtual potential temperature from the domain mean at each vertical level. The buoyancy, velocity variance and vertical velocity of each SCU is calculated over the whole object and then averaged over the lifetime.

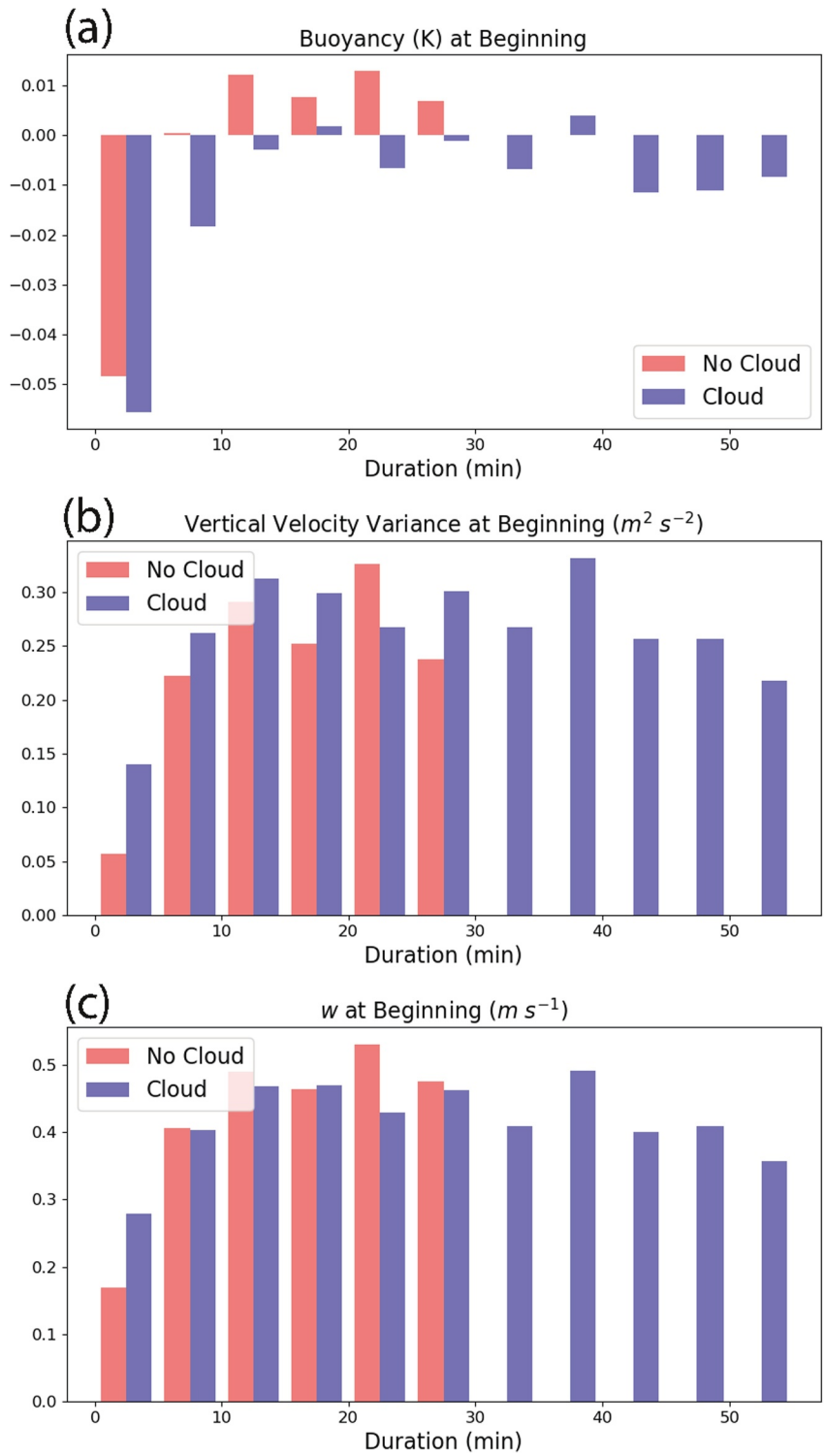

Figure 10. As in Figure 9, but for the initial rather than life-cycle mean properties of sub-cloud coherent updrafts.

lived clouds (less than 5 min) mostly have weak downward cloud-base mass flux. A non-linear increase of cloud lifetime with cloud-base mass flux is consistent with Sakradzija et al. (2015), although their study focused on a precipitating shallow convection case. Our results therefore provide extra evidence to generalize their power law

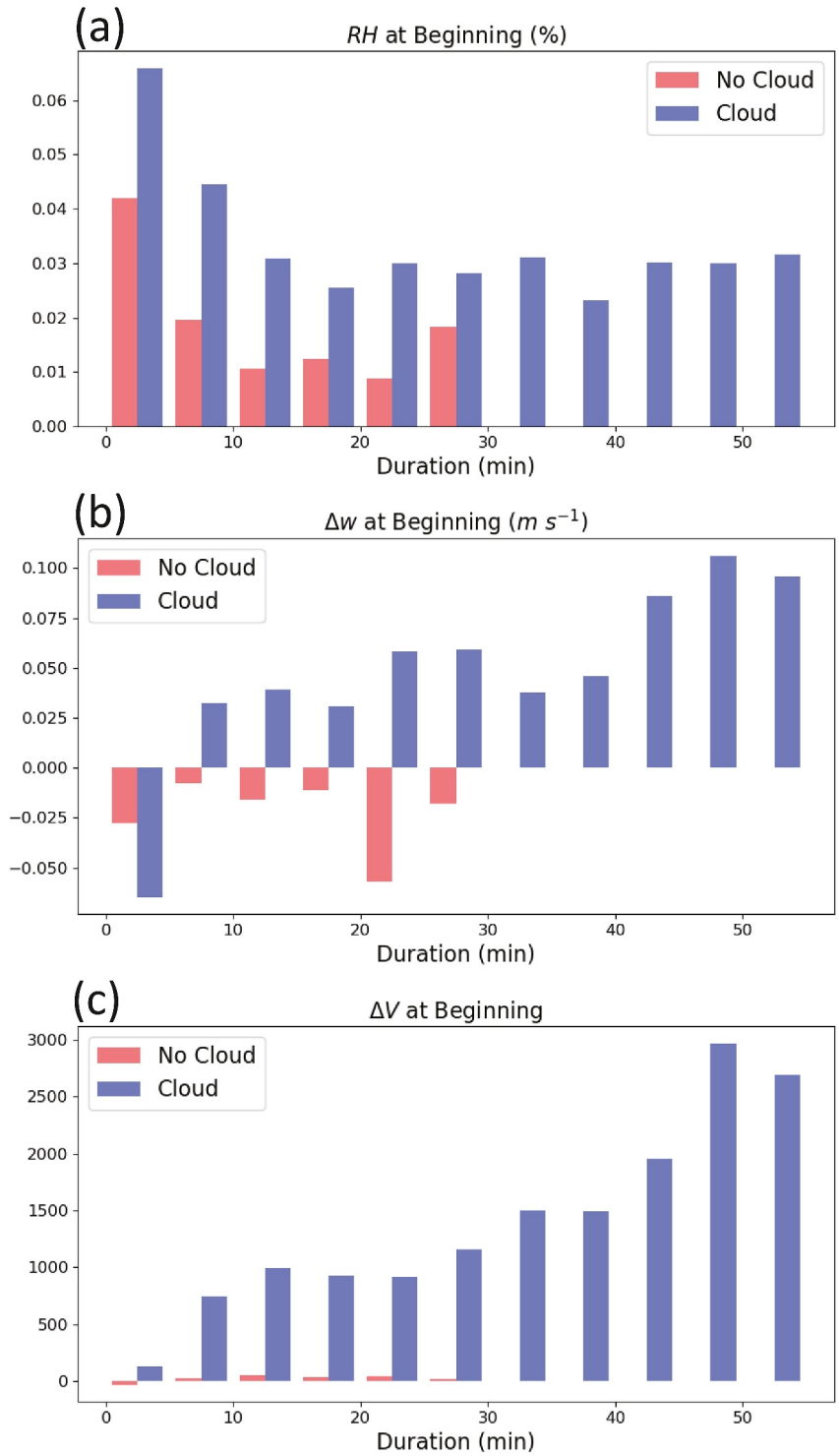

Figure 11. As in Figure 10, but for the initial (a) relative humidity perturbation (%), (b) change of vertical velocity $\left(\mathrm{ms}^{-1}\mathrm{min}^{-1}\right)$ and (c) change of volume of sub-cloud coherent updrafts (number of grid boxes min^{-1}).

empirical relationship between cloud lifetime and cloud-base mass flux for a different type of shallow convection, supporting a unified treatment of cloud lifetime in mass-flux based parameterizations of shallow convection (Sakradzija & Klocke, 2018), though the exact relationship remains elusive and needs further investigations.

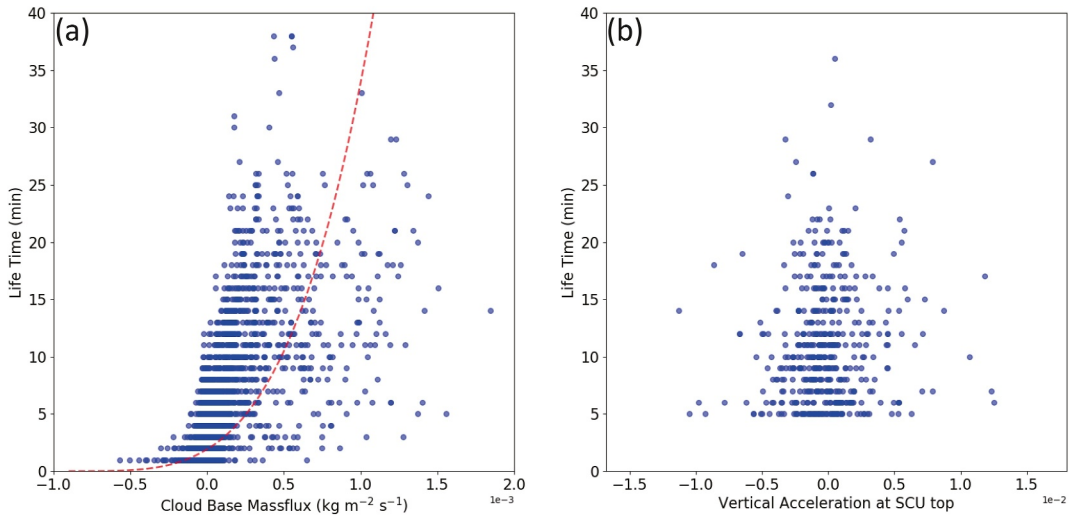

Figure 12. Scatter plots of (a) life-mean cloud-base mass flux and (b) vertical acceleration at the top of the associated sub-cloud coherent updraft (SCU) at the time of cloud initiation, against cloud lifetime. The red dashed line is the fitted line for lifetime (τ) as a function of cloud base mass flux (m): $\tau = \alpha(m + 0.0009)^{\beta}$, for $\alpha = 1.015 \times 10^{12}$, $\beta = 3.85$.

However, the length of cloud lifetime cannot be inferred from the cloud-base mass flux at the time of formation. Recall from Figure 5 that values of the mean cloud-base mass flux in different lifetime groups at the beginning of the cloud life cycle are indistinguishable. Further investigation (not shown) also indicated that both cloud-base area and cloud-base vertical velocity at the time of cloud formation have little relationship to the maintenance of cloud. Thermodynamic conditions, for example, the buoyancy at the time of formation, do not provide useful predictive information either. It is plausible to hypothesize that cloud lifetime might be related to the development of the sub-cloud updraft that is the precursor for a given cloud. With this idea in mind, we consider whether the vertical acceleration of the sub-cloud coherent structure at cloud base at the time of cloud formation might capture the potential for future dynamical support from sub-cloud layer. Although the scatter is large, Figure 12b shows some correlation, with larger vertical acceleration from the sub-cloud coherent structure favoring longer future cloud lifetime. The results here suggest that measures of the development potential of sub-cloud coherent structures could be a possible predictor for the length of cloud lifetime. Given the relatively large scatter and uncertainties, further investigation of this possibility would require the analysis of a range of shallow cumulus simulations and so lies outside the scope of the present study.

7. Summary and Discussion

Observations have shown that shallow cumulus clouds are related to the activities of sub-cloud coherent structures but the exact physical processes underlying the close connections between the two remain ambiguous, which is one of the barriers to improve the parameterization of cloud-subcloud coupling in the numerical models (e.g., Albright et al., 2022; Maason-Delmotte et al., 2021; Sherwood et al., 2014; Vial et al., 2017). Comprehensive understanding of the coupling between the shallow cumulus clouds and sub-cloud layer requires some knowledge of the role of sub-cloud processes in the cloud life cycle. Using a high resolution large eddy simulation and object tracking algorithms, this study takes a step forward to illustrate how sub-cloud energetic coherent structures can govern the formation, development and dissipation of shallow clouds, as summarized in Figure 13.

It is well recognized that sub-cloud coherent structures do not always lead to the formation of clouds, but under what conditions the sub-cloud coherent structures lead to cloud formation is not clear yet (Lareau et al., 2018; LeMone et al., 2019). Our results suggest that the fastest growing coherent structures within a relatively moist region, not the ones with most buoyancy, are more likely to overshoot the LCL and initiate the life cycle of a shallow cloud. Short-lived clouds decay quickly after initiation, most likely due to a disconnection of the sub-cloud coherent structure. The mid- and long-lived clouds go through a distinct development stage, with their cloud-base TKE and mass flux increasing, consistent with the growing strength of the sub-cloud coherent structure. The cloud top rises during this stage. These clouds are continuously supported from below until the sub-

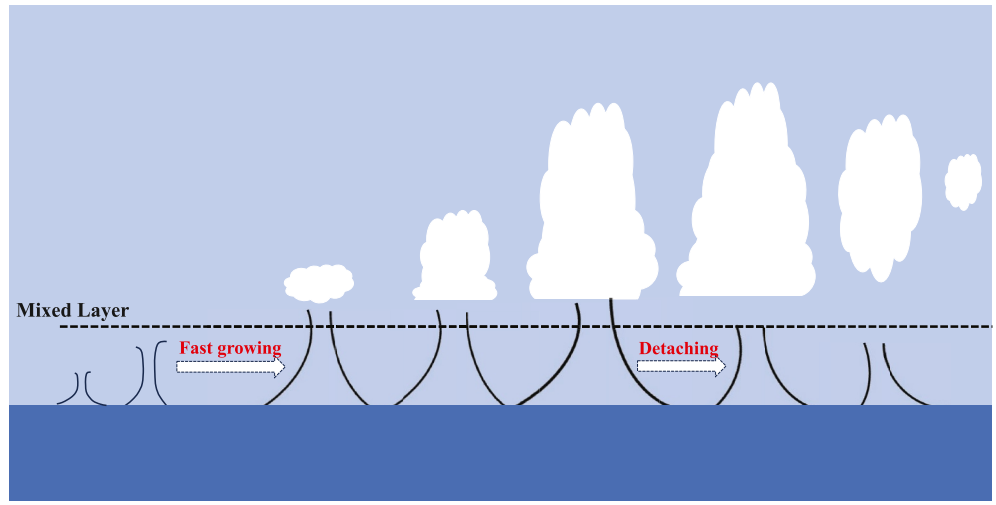

Figure 13. Schematic diagram of the life cycle of shallow trade wind cumulus clouds in relation to the sub-cloud coherent updrafts. Time moves from left to right through the diagram. Dark blue shading marks the ocean. Each pair of black curved lines within the mixed layer represents a sub-cloud coherent updraft (SCU). The width of these curved lines represents the strength of sub-cloud updraft. The white colors represent the clouds. Fast growing SCUs are most likely to trigger the formation of clouds. The level of cloud base keeps steady as the cloud top quickly ascends during the development stage. The cloud base starts to rise and the cloud top starts to lower after the SCU begins to decay and detaches from the lifting condensation level. The cloud dissipates when the cloud top and cloud base approach each other. The horizontal black dashed line marks the top of the mixed layer.

cloud structure becomes detached from the LCL. From this point the cloud base starts to rise and the cloud-base mass flux starts to decrease. The rise of cloud base is a key signature to indicate the beginning of cloud dissipation, after which the cloud top starts to lower. The cloud ends its life cycle as the cloud top and cloud base approach (Heus & Seifert, 2013; Romps et al., 2021; Zhao & Austin, 2005a, 2005b). How long the shallow clouds last after triggering is largely controlled by the life-cycle mean cloud-base mass flux, consistent with Sakradzija et al. (2015). The vertical acceleration of the sub-cloud structure at cloud base is the metric from the initiation time that we found most relevant for indicating future development and the length of lifetime, though the relationship remains elusive.

Observations and high-resolution simulations have identified the critical role of SCUs on the evolution of shallow clouds (LeMone & Pennell, 1976; Lareau et al., 2018; van Stratum et al., 2014; Wang et al., 2022) but very few have provided a continuous framework to encompass the whole physical picture. To our best knowledge, this study is the first to demonstrate explicit evidence to indicate how the life cycle of shallow cumulus clouds is controlled by the sub-cloud coherent structures, continuously from the initiation to the dissipation, providing insights toward improving the representation of boundary layer clouds for further development of convection parameterization. It is suggested that the initiation of shallow clouds does not depend much on whether the initial or life-cycle mean buoyancy of SCUs is positive. Dynamical support, such as the initial vertical velocity variance, and the potential for vertical acceleration, combined with a relatively moist region, are much more important to initiate a cloud. For a mass-flux based parameterization, introducing the life cycle of clouds means that the time evolution of cloud-base mass flux is needed. The simplest treatment is to assume a symmetric function with respect to the middle of the lifetime, as is experimented with in previous studies (Sakradzija & Klocke, 2018; Sakradzija et al., 2015). This representation might not be universal for clouds with different lengths of lifetime. Our results suggest that the longer a cloud lives, the later within the lifetime that the cloud ends its growing phase. Long-lived clouds do tend to achieve the strongest cloud-base mass flux around the mid-point of their lifetime while mid-lived clouds have their maximum cloud-base mass flux ahead of the mid-point of their life cycle. The idea of incorporating the cloud life cycle can also be applied in spectral based convection schemes (Angevine et al., 2020; Neggers, 2015; Neggers & Griewank, 2022; Olson et al., 2019), in which the clouds are sorted on their size. Figure 5b shows that longer-lived clouds are associated with larger life-mean cloud area. This suggests that, the asymmetric evolution of cloud-base mass flux for mid-lived and long-lived clouds can be achieved in a

spectral scheme through including a dependence of cloud lifetime on cloud size. This study further suggests that a lack of cloud at the LCL does not imply the death of a shallow cumulus cloud, which is rather manifest as the approach of cloud top and cloud base. The clouds persist for a while after the rise of cloud base, but before cloud-base mass flux has decayed to zero.

Finally, it should be emphasized that the BOMEX case investigated in this study is a non-precipitating oceanic case. The results from the steady-state BOMEX case cannot necessarily be generalized to other cases of shallow cumulus clouds with diurnal cycle and precipitation. BOMEX has relatively simple large-scale forcing and cloud microphysics, and the basic character of the coupling elucidated between the sub-cloud coherent structure and cloud life cycle may be expected to hold in other cases, although perhaps modified in some ways. The effects of varying forcings or the interaction between dynamics and other microphysical processes can be examined through extending the method developed in this study to analyze other golden cases, such as ARM (A. R. Brown et al., 2002) and RICO (vanZanten et al., 2011), but this will be left for future explorations. The methodology developed in this study can be easily extended to such cases. Efforts are also needed to establish to what extent the results in this study can be generalized to shallow clouds over land or to deep clouds when further processes (e.g., ice microphysics, topographic forcing) become involved. Observational evidence is required to verify whether the pathway described for sub-cloud coherent structures affecting the life cycle of clouds in a large-eddy model is a reasonable representation of what happens in the real atmosphere. In addition to the sub-cloud and cloud interaction, J. Chen et al. (2023) recently suggested that the cloud-cloud interaction can modulate the evolution of the life cycle of shallow cumulus clouds in the U.S. southern Great Plains. Whether such interaction also exists between the sub-cloud coherent structures and indirectly affects the cloud life cycle through the feedback on the cloud-cloud interaction is of great interest and worthy of future investigation.

Conflict of Interest

The authors declare no conflicts of interest relevant to this study.

Data Availability Statement

The data from the large eddy simulation used for the analyses in this study is publicly available in the Zenodo repository (Gu, Plant, & Holloway, 2024) (https://zenodo.org/record/8300016).

Acknowledgments
This work is funded by NERC under the joint NERC/Met Office ParaCon programme, specifically through the ParaCon Phase 2 project, NE/T003871/1. J. F. Gu is also supported through National Natural Science Foundation of China under Grants 42192555 and the Fundamental Research Funds for the Central Universities 0207/14380225, 0207/14912209. We gratefully acknowledge Adrian Hill, Nick Brown and Todd Jones for their support of the Met Office/NERC Cloud model (MONC). The simulation was conducted on Monsoon2, a collaborative High Performance Computing facility funded by the Met Office and NERC, and the analyses were conducted on the NERC/NCAS (National Center for Atmospheric Science) JASMIN computer facility. Finally, we would like to acknowledge Professor Roel Neggers and two anonymous reviewers for their constructive comments that help improve the manuscript.

References

Albright, A. L., Bony, S., Stevens, B., & Vogel, R. (2022). Observed subcloud-layer moisture and heat budgets in the trades. *Journal of the Atmospheric Sciences*, *79*(9), 2363–2385. https://doi.org/10.1175/JAS-D-21-0337.1

Angevine, W. M., Olson, J., Gristey, J. J., Glenn, I., Feingold, G., & Turner, D. D. (2020). Scale awareness, resolved circulations, and practical limits in the MYNN-EDMF boundary layer and shallow cumulus scheme. *Monthly Weather Review*, *148*(11), 4629–4639. https://doi.org/10.1175/MWR-D-20-0066.1

Betts, A. K. (1973). Non-precipitating cumulus convection and its parameterization. *Quarterly Journal of the Royal Meteorological Society*, *99*(419), 178–196. https://doi.org/10.1002/qj.49709941915

Blyth, A. M., Lasher-Trapp, S. G., & Cooper, W. A. (2005). A study of thermals in cumulus clouds. *Quarterly Journal of the Royal Meteorological Society*, *131*(607), 1171–1190. https://doi.org/10.1256/qj.03.180

Bony, S., & Dufresne, J.-L. (2005). Marine boundary layer clouds at the heart of tropical cloud feedback uncertainties in climate models. *Geophysical Research Letters*, *32*(20), L20806. https://doi.org/10.1029/2005GL023851

Brient, F., Schneider, T., Tan, Z., Bony, S., Qiu, X., & Hall, A. (2016). Shallowness of tropical low clouds as a predictor of climate models' response to warming. *Climate Dynamics*, *47*(1–2), 433–449. https://doi.org/10.1007/s00382-015-2846-0

Brown, A. R., Cederwall, R. T., Chlond, A., Duynkerke, P. G., Golaz, J.-C., Khairoutdinov, M., et al. (2002). Large-eddy simulation of the diurnal cycle of shallow cumulus convection over land. *Quarterly Journal of the Royal Meteorological Society*, *128*(582), 1075–1093. https://doi.org/10.1256/003590002320373210

Brown, N., Lepper, A., Weiland, M., Hill, A., & Shipway, B. (2018). In situ data analytics for highly scalable cloud modelling on cray machines. *Concurrency and Computation: Practice and Experience*, *30*(1), e4331. https://doi.org/10.1256/qj.04.101

Brown, N., Lepper, A., Weiland, M., Hill, A., Shipway, B., Maynard, C., et al. (2015). A highly scalable Met Office NERC Cloud model. In *Proceedings of the 3rd international conference on exascale applications and software-EASC 2015* (pp. 132–137).

Chen, J., Hagos, S., Feng, Z., Fast, J. D., & Xiao, H. (2023). The role of cloud-cloud interaction in the life cycle of shallow cumulus clouds. *Journal of the Atmospheric Sciences*, *80*(3), 671–686. https://doi.org/10.1175/JAS-D-22-0004.1

Chen, S. S., & Houze, R. A., Jr. (1997). Diurnal variation and life-cycle deep convective systems over the tropical pacific warm pool. *Quarterly Journal of the Royal Meteorological Society*, *123*(538), 357–388. https://doi.org/10.1002/qj.49712353806

Cho, H.-R. (1977). Contributions of cumulus cloud life-cycle effects to the large-scale heat and moisture budget equations. *Journal of the Atmospheric Sciences*, *34*(1), 87–97. https://doi.org/10.1175/1520-0469(1977)034⟨0087:COCCLC⟩2.0.CO;2

Couvreux, F., Hourdin, F., & Rio, C. (2010). Resolved versus parameterized boundary-layer plumes. Part I: A parameterization-oriented conditional sampling in large-eddy simulations. *Boundary-Layer Meteorology*, *134*(3), 441–458. https://doi.org/10.1007/s10546-009-9456-5

Dawe, J. T., & Austin, P. H. (2012). Statistical analysis of an les shallow cumulus cloud ensemble using a cloud tracking algorithm. *Atmospheric Chemistry and Physics*, *12*(2), 1101–1119. https://doi.org/10.5194/acp-12-1101-2012

Denby, L., Böing, S. J., Parker, D. J., Ross, A. N., & Tobias, S. M. (2022). Characterising the shape, size, and orientation of cloud-feeding coherent boundary-layer structures. *Quarterly Journal of the Royal Meteorological Society*, *148*(742), 499–519. https://doi.org/10.1002/qj.4217

Endo, S., Zhang, D., Vogelmann, A. M., Kollias, P., Lamer, K., Oue, M., et al. (2019). Reconciling differences between large-eddy simulations and Doppler Lidar observations of continental shallow cumulus cloud-base vertical velocity. *Geophysical Research Letters*, *46*(20), 11539–11547. https://doi.org/10.1029/2019GL084893

Fletcher, J. K., & Bretherton, C. S. (2010). Evaluating boundary layer-based mass flux closures using cloud-resolving model simulations of deep convection. *Journal of the Atmospheric Sciences*, *67*(7), 2212–2225. https://doi.org/10.1175/2010jas3328.1

Golaz, J.-C., Larson, V. E., & Cotton, W. R. (2002). A pdf-based model for boundary layer clouds. Part I: Method and model description. *Journal of the Atmospheric Sciences*, *59*(24), 3540–3551. https://doi.org/10.1175/1520-0469(2002)059⟨3540:APBMFB⟩2.0.CO;2

Grant, A. L. M. (2006). The cumulus-capped boundary layer. II: Interface fluxes. *Quarterly Journal of the Royal Meteorological Society*, *132*(618), 1405–1422. https://doi.org/10.1256/qj.04.170

Gregory, D., & Rowntree, P. R. (1990). A mass flux convection scheme with representation of cloud ensemble characteristics and stability-dependent closure. *Monthly Weather Review*, *118*(7), 1483–1506. https://doi.org/10.1175/1520-0493(1990)118⟨1483:AMFCSW⟩2.0.CO;2

Griewank, P. J., Heus, T., Lareau, N. P., & Neggers, R. A. J. (2020). Size dependence in chord characteristics from simulated and observed continental shallow cumulus. *Atmospheric Chemistry and Physics*, *20*(17), 10211–10230. https://doi.org/10.5194/acp-20-10211-2020

Griewank, P. J., Heus, T., & Neggers, R. A. J. (2022). Size-dependent characteristics of surface-rooted three-dimensional convective objects in continental shallow cumulus simulations. *Journal of Advances in Modeling Earth Systems*, *14*(3), 2021MS002612. https://doi.org/10.1029/2021MS002612

Gu, J.-F., Plant, R. S., & Holloway, C. E. (2024a). Connections between sub-cloud coherent structures and the life cycle of maritime shallow cumulus clouds in large eddy simulation. [Dataset]. *Zenodo*. https://zenodo.org/record/8300016

Gu, J.-F., Plant, R. S., Holloway, C. E., & Clark, P. A. (2024b). The moist halo region around shallow cumulus clouds in large eddy simulations. *Quarterly Journal of the Royal Meteorological Society*, *150*(760), 1501–1517. https://doi.org/10.1002/qj.4656

Gu, J.-F., Plant, R. S., Holloway, C. E., & Muetzelfeldt, M. (2020). Pressure drag for shallow cumulus clouds: From thermals to the cloud ensemble. *Geophysical Research Letters*, *47*(22), e2020GL090460. https://doi.org/10.1029/2020GL090460

Heus, T., Jonker, H. J. J., den Akker, H. E. A. V., Griffith, E. J., Koutek, M., & Post, F. H. (2009). A statistical approach to the life cycle analysis of cumulus clouds selected in a virtual reality environment. *Journal of Geophysical Research*, *114*(D6), D06208. https://doi.org/10.1029/2008JD010917

Heus, T., & Seifert, A. (2013). Automated tracking of shallow cumulus clouds in large domain. *Geoscientific Model Development*, *6*(4), 1261–1273. https://doi.org/10.5194/gmd-6-1261-2013

Jiang, H., Xue, H., Teller, A., Feingold, G., & Levin, Z. (2006). Aerosol effects on the lifetime of shallow cumulus. *Geophysical Research Letters*, *33*(14), L14806. https://doi.org/10.1029/2006GL026024

Kain, J. S. (2004). The Kain-Fritsch convective parameterization: An update. *Journal of Applied Meteorology and Climatology*, *43*(1), 170–181. https://doi.org/10.1175/1520-0450(2004)043⟨0170:TKCPAU⟩2.0.CO;2

Kairoutdinov, M. F., & Randall, D. A. (2002). Similarity of deep continental cumulus convection as revealed by a three-dimensional cloud-resolving model. *Journal of the Atmospheric Sciences*, *59*(17), 2550–2566. https://doi.org/10.1175/1520-0469(2002)059⟨2550:SODCCC⟩2.0.CO;2

Kuang, Z., & Bretherton, C. S. (2006). A mass-flux scheme view of a hgih-resolution simulation of a transition from shallow to deep cumulus convection. *Journal of the Atmospheric Sciences*, *63*(7), 1895–1909. https://doi.org/10.1175/JAS3723.1

Lareau, N. P., Zheng, Y., & Klein, S. A. (2018). Observed boundary layer controls on shallow cumulus at the arm southern Great Plains site. *Journal of the Atmospheric Sciences*, *75*(7), 2235–2255. https://doi.org/10.1175/jas-d-17-0244.1

Larson, V. E. (2017). Clubb-Silhs: A parameterization of subgrid variability in the atmosphere. *arXiv*. https://doi.org/10.48550/arXiv.1711.03675

Larson, V. E., & Golaz, J.-C. (2005). Using probability density functions to derive consistent closure relationships among higher-order moments. *Monthly Weather Review*, *133*(4), 1023–1042. https://doi.org/10.1175/MWR2902.1

Larson, V. E., Golaz, J.-C., & Cotton, W. R. (2002). Small-scale and mesoscale variability of scalars in cloudy boundary layers: Joint probability density functions. *Journal of the Atmospheric Sciences*, *59*(24), 3519–3539. https://doi.org/10.1175/1520-0469(2002)059⟨3519:SSAMVI⟩2.0.CO;2

LeMone, M. A., Angevine, W. M., Bretherton, C. S., Chen, F., Dudhia, J., Fedorovich, E., et al. (2019). 100 years of progress in boundary layer meteorology. *Meteorological Monographs*, *59*, 9.1–9.85. https://doi.org/10.1175/AMSMONOGRAPHS-D-18-0013.1

LeMone, M. A., & Pennell, W. T. (1976). The relationship of trade wind cumulus distribution to subcloud layer fluxes and structure. *Monthly Weather Review*, *104*(5), 524–539. https://doi.org/10.1175/1520-0493(1976)104⟨0524:TROTWC⟩2.0.CO;2

Lilly, D. K. (1962). On the numerical simulation of buoyant convection. *Tellus*, *14*(2), 2153–3490. https://doi.org/10.1111/j.2153-3490.1962.tb00128.x

Maason-Delmotte, V., Zhai, P., Pirani, A., Connors, S. L., Péan, C., Berger, S., et al (Eds.) (2021). *Ipcc, 2021: Climate change 2021: The physical science basis*. Cambridge University Press. https://doi.org/10.1017/9781009157896

Muetzelfeldt, M. (2020). Designs for representing shear-induced cloud field organization in a convection parametrization scheme. PhD thesis. *Department of Meteorology, University of Reading*, 245.

Neggers, R. A. J. (2015). Exploring bin-macrophysics models for moist convective transport and clouds. *Journal of Advances in Modeling Earth Systems*, *7*(4), 2079–2104. https://doi.org/10.1002/2015MS000502

Neggers, R. A. J., & Griewank, P. J. (2021). A binomial stochastic framework for efficiently modeling discrete statistics of convective populations. *Journal of Advances in Modeling Earth Systems*, *13*(3), e2020MS002229. https://doi.org/10.1029/2020MS002229

Neggers, R. A. J., & Griewank, P. J. (2022). A decentralized approach for modeling organized convection based on thermal populations on microgrids. *Journal of Advances in Modeling Earth Systems*, *14*(10), e2022MS003042. https://doi.org/10.1029/2022MS003042

Neggers, R. A. J., Jonker, H. J. J., & Siebesma, A. P. (2003). Size statistics of cumulus cloud populations in large-eddy simulations. *Journal of the Atmospheric Sciences*, *60*(8), 1060–1074. https://doi.org/10.1175/1520-0469(2003)60⟨1060:SSOCCP⟩2.0.CO;2

Neggers, R. A. J., Stevens, B., & Neelin, J. D. (2006). A simple equilibrium model for shallow-cumulus-topped mixed layers. *Theoretical and Computational Fluid Dynamics*, *20*(5–6), 305–322. https://doi.org/10.1007/s00162-006-0030-1

Nicholls, S., & LeMone, M. A. (1980). The fair weather boundary layer in gate: The relationship of subcloud fluxes and structure to the distribution and enhancement of cumulus clouds. *Journal of the Atmospheric Sciences*, *37*(9), 2051–2067. https://doi.org/10.1175/1520-0469(1980)037⟨2051:TFWBLI⟩2.0.CO;2

Öktem, R., Prabhat, M., Lee, J., Thomas, A., Zuidema, P., & Romps, D. M. (2014). Stereo photogrammetry of oceanic clouds. *Journal of Atmospheric and Oceanic Technology*, *41*(7), 1482–1502. https://doi.org/10.1175/jtech-d-13-00224.1

Olson, J. B., Kenyon, J. S., Angevine, W. M., Brown, J. M., Pagowski, M., & Suselj, K. (2019). A description of the MYNN–EDMF scheme and coupling to other components in WRF-ARW. *NOAA Tech. Memo., OAR GSD-61, 42*.

Plant, R. S. (2009). Statistical properties of cloud lifecycles in cloud-resolving models. *Atmospheric Chemistry and Physics*, *9*(6), 2195–2205. https://doi.org/10.5194/acp-9-2195-2009

Rio, C., & Hourdin, F. (2008). A thermal plume model for the convective boundary layer: Representation of cumulus clouds. *Journal of the Atmospheric Sciences*, *65*(2), 407–425. https://doi.org/10.1175/2007JAS2256.1

Romps, D. M., & Öktem, R. (2018). Observing clouds in 4d with multiview stereophotogrammetry. *Bulletin of the American Meteorological Society*, *99*(12), 2575–2586. https://doi.org/10.1175/bams-d-18-0029.1

Romps, D. M., Öktem, R., Endo, S., & Vogelmann, A. M. (2021). On the lifecycle of a shallow cumulus cloud: Is it a bubble or plume, active or forced? *Journal of the Atmospheric Sciences*, *78*(9), 2823–2833. https://doi.org/10.1175/jas-d-20-0361.1

Sakradzija, M., & Klocke, D. (2018). Physically constrained stochastic shallow convection in realistic kilometer-scale simulations. *Journal of Advances in Modeling Earth Systems*, *10*(11), 2755–2776. https://doi.org/10.1029/2018MS001358

Sakradzija, M., Seifert, A., & Heus, T. (2015). Fluctuations in a quasi-stationary shallow cumulus cloud ensemble. *Nonlinear Processes in Geophysics*, *22*(1), 65–85. https://doi.org/10.5194/npg-22-65-2015

Scorer, R. S., & Ludlam, F. H. (1953). Bubble theory of penetrative convection. *Quarterly Journal of the Royal Meteorological Society*, *79*(339), 94–103. https://doi.org/10.1002/qj.49707933908

Seelig, T., Deneke, H., Quaas, J., & Tesche, M. (2021). Life cycle of shallow marine cumulus clouds from geostationary satellite observations. *Journal of Geophysical Research: Atmospheres*, *126*(22), e2021JD035577. https://doi.org/10.1029/2021JD035577

Sherwood, S., Bony, S., & Dufresne, J.-L. (2014). Spread in model climate sensitivity traced to atmospheric convective mixing. *Nature*, *505*(7481), 31–42. https://doi.org/10.1038/nature12829

Siebesma, A. P., Bretherton, C. S., Brown, A., Chlond, A., Cuxart, J., Duynkerke, P. G., et al. (2003). A large eddy simulation intercomparison study of shallow cumulus convection. *Journal of the Atmospheric Sciences*, *60*(10), 1201–1219. https://doi.org/10.1175/1520-0469(2003)60,1201:ALESIS.2.0.CO;2

Siebesma, A. P., & Cuijpers, J. W. M. (1995). Evaluation of parametric assumptions for shallow cumulus convection. *Journal of the Atmospheric Sciences*, *52*(6), 650–666. https://doi.org/10.1175/1520-0469(1995)052⟨0650:EOPAFS⟩2.0.CO;2

Siebesma, A. P., & Jonker, H. J. J. (2000). Anomalous scaling of cumulus cloud boundaries. *Physical Review Letters*, *85*(1), 214–217. https://doi.org/10.1103/PhysRevLett.85.214

Siebesma, A. P., Soares, P. M. M., & Teixeira, J. (2007). A combined eddy-diffusivity mass-flux approach for the convective boundary layer. *Journal of the Atmospheric Sciences*, *64*(4), 1230–1248. https://doi.org/10.1175/JAS3888.1

Smagorinsky, J. (1963). General circulation experiments with the primitive equation: I. The basic experiment. *Monthly Weather Review*, *91*(3), 99–164. https://doi.org/10.1175/1520-0493(1963)091⟨0099:GCEWTP⟩2.3.CO;2

Soares, P. M. M., Miranda, P. M. A., Siebesma, A. P., & Teixeira, J. (2004). An eddy-diffusivity/mass-flux parameterization for dry and shallow cumulus convection. *Quarterly Journal of the Royal Meteorological Society*, *130*, 3365–3384. https://doi.org/10.1256/qj.03.223

Stein, T. H. M., Hogan, R. J., Hanley, K. E., Nicol, J. C., Lean, H. W., Plant, R. S., et al. (2014). The three-dimensional morphology of simulated and observed convective storms over southern england. *Monthly Weather Review*, *142*(9), 3264–3283. https://doi.org/10.1175/MWR-D-13-00372.1

Stevens, B. (2006). Bulk boundary-layer concepts for simplified models of tropical dynamics. *Theoretical and Computational Fluid Dynamics*, *20*(5–6), 279–304. https://doi.org/10.1007/s00162-006-0032-z

Suselj, K., Kurowski, M. J., & Teixeira, J. (2019). A unified eddy-diffusivity/mass-flux approach for modeling atmospheric convection. *Journal of the Atmospheric Sciences*, *76*(8), 2505–2537. https://doi.org/10.1175/JAS-D-18-0239.1

Suselj, K., Teixeira, J., & Metheou, G. (2012). Eddy diffusivity/mass flux and shallow cumulus boundary layer: An updraft pdf multiple mass flux scheme. *Journal of the Atmospheric Sciences*, *69*, 1513–1533. https://doi.org/10.1175/JAS-D-11-090.1

Tan, Z., Kaul, C. M., Pressel, K. G., Cohen, Y., Schneider, T., & Teixeira, J. (2018). An extended eddy-diffusivity mass-flux scheme for unified representation of subgrid-scale turbulence and convection. *Journal of Advances in Modeling Earth Systems*, *10*(3), 770–800. https://doi.org/10.1002/2017MS001162

van Stratum, B. J. H., de Arellano, J. V., van Heervaarden, C. C., & Ouwersloot, H. G. (2014). Subcloud-layer feedbacks driven by the mass flux of shallow cumulus convection over land. *Journal of the Atmospheric Sciences*, *71*(3), 881–895. https://doi.org/10.1175/JAS-D-13-0192.1

van Zanten, M. C., Stevens, B., Nuijens, L., Siebesma, A. P., Ackerman, A. S., Burnet, F., et al. (2011). Controls on precipitation and cloudiness in simulations of trade-wind cumulus as observed during Rico. *Journal of Advances in Modeling Earth Systems*, *3*(2), M06001. https://doi.org/10.1029/2011MS000056

Vial, J., Bony, S., Dufresne, J.-L., & Roehrig, R. (2016). Coupling between lower-tropospheric convective mixing and low-level clouds: Physical mechanisms and dependence on convection scheme. *Journal of Advances in Modeling Earth Systems*, *8*(4), 1892–1911. https://doi.org/10.1002/2016MS000740

Vial, J., Bony, S., Stevens, B., & Vogel, R. (2017). Mechanisms and model diversity of trade-wind shallow cumulus cloud feedbacks: A review. *Surveys in Geophysics*, *38*(6), 1331–1353. https://doi.org/10.1007/s10712-017-9418-2

Vial, J., Dufresne, J.-L., & Bony, S. (2013). On the interpretation of inter-model spread in CMIP5 climate sensitivity estimates. *Climate Dynamics*, *41*(11–12), 3339–3362. https://doi.org/10.1007/s00382-013-1725-9

Wang, Y., Cheng, X., Fei, J., & Zhou, B. (2022). Modeling the shallow cumulus-topped boundary layer at gray zone resolutions. *Journal of the Atmospheric Sciences*, *79*(9), 2435–2451. https://doi.org/10.1175/JAS-D-21-0339.1

Williams, A. G., Zahorowski, W., Chambers, S., Griffiths, A., Hacker, J. M., Element, A., et al. (2011). The vertical distribution of radon in clear and cloudy daytime terrestrial boundary layers. *Journal of the Atmospheric Sciences*, *68*(1), 155–174. https://doi.org/10.1175/2010JAS3576.1

Xie, S., Zhang, M., Boyle, J. S., Cederwall, R. T., Potter, G. L., & Lin, W. (2004). Impact of a revised convective triggering mechanism on Community Atmosphere Model, Version 2, simulations: Results from short-range weather forecasts. *Journal of Geophysical Research*, *109*(D14), D14102. https://doi.org/10.1029/2004JD004692

Zelinka, M. D., Myers, T. A., McCoy, D. T., Po-Chedley, S., Caldwell, P. M., Ceppi, P., et al. (2020). Causes of higher climate sensitivity in CMIP6 models. *Geophysical Research Letters*, *47*(1), e2019GL085782. https://doi.org/10.1029/2019GL085782

Zhang, Y., Klein, S. A., Fan, J., Chandra, A. S., Kollias, P., Xie, S., & Tang, S. (2017). Large-eddy simulation of shallow cumulus over land: A composite case based on arm long-term observations at its southern Great Plains site. *Journal of the Atmospheric Sciences*, *74*(10), 3229–3251. https://doi.org/10.1175/JAS-D-16-0317.1

Zhao, M., & Austin, P. H. (2005a). Life cycle of numerically simulated shallow cumulus clouds. Part II: Mixing dynamics. *Journal of the Atmospheric Sciences*, *62*(5), 1291–1310. https://doi.org/10.1175/JAS3415.1

Zhao, M., & Austin, P. H. (2005b). Life cycle of numerically simulated shallow cumulus clouds. Part I: Transport. *Journal of the Atmospheric Sciences*, *62*(5), 1269–1290. https://doi.org/10.1175/JAS3414.1

Zheng, Y. (2019). Theoretical understanding of the linear relationship between convective updrafts and cloud-base height for shallow cumulus clouds. Part I: Maritime conditions. *Journal of the Atmospheric Sciences*, *76*(8), 2539–2558. https://doi.org/10.1175/JAS-D-18-0323.1

Zheng, Y., Rosenfeld, D., & Li, Z. (2021). Sub-cloud turbulence explains cloud-base updrafts for shallow cumulus ensembles: First observational evidence. *Geophysical Research Letters*, *48*(6), e2020GL091881. https://doi.org/10.1029/2020GL091881